Geomechanics and Engineering, *Vol. 42, No. 2 (2025) 129-145*
https://doi.org/10.12989/gae.2025.42.2.129

A simple algorithm for predicting the maximum surface settlement considering support mechanisms of shield tunneling

Jun-Beom An[1a], Seok-Jun Kang[2b] and Gye-Chun Cho*[1]

[1]*Department of Civil and Environmental Engineering, Korea Advanced Institute of Science and Technology, 291 Daehak-ro, Yuseong-gu, Daejeon 34141, Republic of Korea*
[2]*Department of Geosciences, Texas Tech University, Lubbock, TX 79409, United States*

(*Received January 9, 2025, Revised July 3, 2025, Accepted July 4, 2025*)

Abstract. Accurate prediction of ground surface settlement is essential in urban shield tunneling projects to prevent damage to nearby structures. While empirical and data-driven models have been widely used, they often neglect support mechanisms such as grouting and slurry injection, or require extensive datasets that are not always available to obtain promptly. This study proposes a simple and practical algorithm for predicting the maximum surface settlement induced by shield tunneling. The algorithm was developed using the parametric results from three-dimensional numerical modeling of the excavation and support process of shield Tunnel Boring Machines (TBMs). The results indicated that the stiffness of the weaker support material plays a dominant role in controlling settlement, particularly when the face pressure is maintained above the active earth pressure. For the purpose of incorporating the effects of support mechanisms, three gap parameters were defined at the tunnel face, shield annular gap, and tail void, and were modified based on stress states and support stiffness. Correction coefficients were introduced to quantify the contribution of each support phase at specific ground type. The proposed algorithm requires only a limited number of input variables, such as ground properties and face pressure, making it suitable for field application. The model was validated against field measurements with prediction errors within 2 mm. This study provides a physically grounded and computationally efficient framework that improves predictive accuracy while addressing limitations of traditional methods in shield tunneling settlement analysis.

Keywords: earth pressure; numerical analyses; settlement; tunnel; tunnelling

1. Introduction

Excavation of tunnels in urban areas often involves their proximity to existing structures and the impact on the surrounding ground. As an efficient tunneling method with minimal disturbance, the Tunnel Boring Machine (TBM), especially Shield TBM, has been widely adopted for urban underground works. Nevertheless, the tunneling process inevitably disturbs the initial stress state of the ground, potentially causing surface settlements that pose significant risks to the safety of adjacent surface structures. Therefore, it is essential to accurately predict the tunneling-induced surface settlements and implement effective mitigation strategies to protect nearby infrastructures in a timely manner.

The tunneling-induced surface settlement has been studied extensively through various approaches, including observational data analysis (Peck 1969, Standing and Selemetas 2013, Wan *et al.* 2017), theoretical analysis (Dalong *et al.* 2020, Loganathan and Poulos 1998, Verruijt and Booker 1996), and physical model testing (Chapman *et al.* 2007, Nomoto *et al.* 1999, Xiang *et al.* 2018). However, these conventional approaches are typically designed for specific tunneling conditions, limiting their ability to capture the complex interactions between shield tunneling and the surrounding ground and thus restricting their general applicability in settlement predictions. In efforts to understand the intricate surface settlement mechanisms related to shield tunneling operations, numerical studies have been widely conducted (Kasper and Meschke 2004, Kasper and Meschke 2006a, Kasper and Meschke 2006b, Lambrughi *et al.* 2012, Mroueh and Shahrour 2008, Ochmański *et al.* 2018). Numerical methods offer distinct advantages, enabling comprehensive simulations and detailed visualizations that account for tunnel face behavior, longitudinal settlement troughs, 3D arching effects, and temporary heave near the excavation front. However, for practical applications, these physics-based models are considered inefficient in predicting settlement due to their high computational costs and the requirement for explicit parameter calibration (Zhang *et al.* 2020). Recently, with advances in computer science and artificial intelligence, several data-driven models have been developed to replace conventional physics-based methods (Goh *et al.* 2018, Zhang *et al.* 2021a). Starting from the conventional artificial neural network (ANN) (Kim *et al.* 2001, Santos Jr and Celestino 2008, Suwansawat and Einstein 2006), various machine learning algorithm are adopted for settlement prediction (Chen *et al.* 2019, Freitag *et al.* 2018,

*Corresponding author, Professor
E-mail: gyechun@kaist.edu
[a]Ph.D.
[b]Ph.D.

ISSN: 2005-307X (Print), 2092-6219 (Online)

Kim *et al.* 2022, Zhang *et al.* 2021b, Zhou *et al.* 2023). However, the application of machine learning to predict shield tunneling-induced settlement still faces significant challenges, such as limited training data, reduced reliability, and limited generalizability, making practical implementation difficult (Karniadakis *et al.* 2021, Phoon and Zhang 2023, Reichstein *et al*. 2019). Thus, overcoming the limitations of existing settlement analysis and prediction methods requires developing models that are computationally efficient, incorporate both environmental and mechanical variables relevant to shield tunneling, and are broadly applicable and reliable across diverse tunneling sites. To address these issues, the semi-empirical prediction model can provide an effective approach (Loganathan 2011). These models, structured using experimental and numerical analysis results that reflect underlying physical mechanisms, are suitable for practical on-site implementation of settlement prediction systems.

In this study, a practical algorithm for predicting maximum surface settlement is proposed using numerical simulation results. The algorithm incorporates gap parameters representing the face stability and deformation of physical gap to integrate the support mechanisms in shield tunneling. To ensure generality and usability, the algorithm is formulated under undrained ground conditions, because the groundwater inflow during the shield tunneling is governed by geological or structural factors than operational support mechanisms. Each gap parameters are modified by integrating stress states and the support stiffness concept from the convergence-confinement method. Additionally, coefficients reflecting the contributions of each support phase to surface settlement are introduced, allowing for a quantitative assessment of settlement mechanisms encountered in actual tunneling. Each coefficient is determined through a simple numerical parametric analysis based on the face pressure, grout and slurry injection pressure, and geotechnical properties, which affect surface settlement depending on the support phase. The proposed prediction algorithm, which requires only basic geotechnical parameters, effectively and accurately estimates maximum surface settlement for shield tunneling in undrained conditions.

2. Development of settlement predictive algorithm

A practical prediction algorithm should be simple enough to be embedded into the excavation management system in the field. In this study, the algorithm is designed to reflect the settlement mechanisms under the operation of shield tunneling in undrained conditions.

The surface settlement induced by the excavation of circular tunnel has been found to vary with factors such as the vertical distance between the tunnel and the depth of interest (Mair *et al.* 1993, Marshall *et al.* 2012, O'Reilly and New 1982), excavated diameter (Attewell and Farmer 1974, Loganathan and Poulos 1998), cover-to-diameter ratio (Sugiyama *et al*. 1999), ground type (Mair and Taylor 1999, Selby 1988), and the magnitude of ground loss (Jacobsz 2002). Settlements caused by tunneling are often quantified

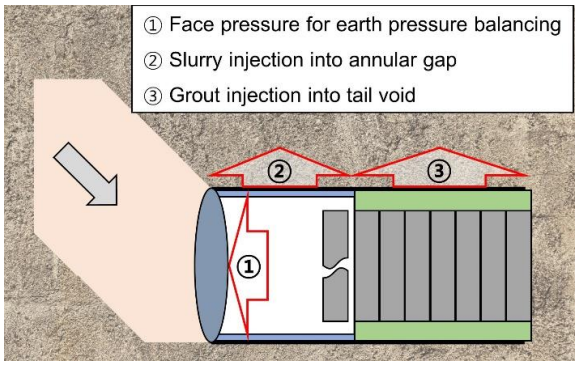

Fig. 1 Schematic of pressurized shield tunneling

using the term ‘volume loss’. It is defined as the transverse settlement trough area, denoted by V_S. The transverse settlement trough is known to match the Gaussian distribution curve (Peck 1969), which can be expressed as

$$S = S_{max} \cdot exp\left(\frac{-x^2}{2i^2}\right) \quad (1)$$

where S_{max} is the maximum surface settlement, i is the horizontal distance from the tunnel centerline to the point of inflection on the settlement trough, and x is the horizontal distance from the tunnel centerline. The area of settlement through V_S, can be evaluated by integrating Eq. (1) to give Eq. (2).

$$V_S = \sqrt{2\pi} \cdot i \cdot S_{max} \quad (2)$$

Also the volume loss is usually expressed as the percentage fraction denoted by V_L, of the tunnel excavation area.

Shield TBM excavates the circular tunnel resulting in a physical gap. Shield machines typically have a tapered geometry with a larger diameter cutterhead, creating a shield annular gap (overcut). The thickness of the overcut, known to vary depending on the TBM type and ground properties, was controlled within the range of 0.02 to 0.15 m (Comodromos *et al*. 2014, Hasanpour 2014, Lambrughi *et al.* 2012, Ramoni and Anagnostou 2010, Repetto and Fidelibus 2017, Zhao *et al.* 2012). The segment lining inside the shield has a smaller diameter than the excavated periphery, creating a gap called the tail void. The volume loss during shield tunneling is quantitatively estimated using a gap parameter (Lee *et al.* 1992, Rowe and Lee 1992). The gap parameter was assumed to be a semi-analytically estimated volume loss considering the tunneling sequence. In large-diameter shield machines, the shield annular gap is typically filled with bentonite slurry, while the tail void is filled with mortar grout. The radial deformation of the support materials providing passive support is empirically incorporated into the gap parameter as modified by Loganathan (2011). Although the injection pressures of the slurry and grout along the excavated periphery can reduce the ground deformation (Mooney *et al.* 2016, Suwansawat and Einstein 2007), these active supports were not considered when using the gap parameter. Fig. 1 illustrates the schematics of annular gaps and support pressures during pressurized shield tunneling.

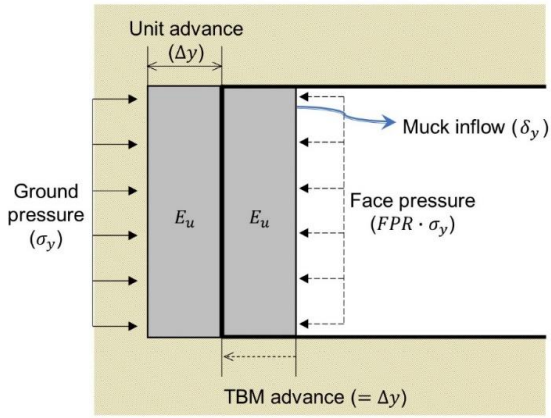

Fig. 2 Schematic of the face support for shield tunneling

This study modifies the gap parameter to reflect those two major support mechanism of shield tunneling. The modified gap parameter on the tunnel face (g_{face}) is defined as the difference between the radius of the equivalent radial ground loss (r_{eq}) and the excavation radius (r), which are regarded as coaxial. It is described by the deformation of the ground in front of the shield face. Fig. 2 illustrates the concept of face support in shield tunneling. If the face pressure (FP) is greater than the total earth pressure (σ_y), the ground would be compressed forward, resulting in less muck discharge. Conversely, if the face pressure is less than the total earth pressure, the ground would be compressed inward, leading to increased ground intrusion. The intrusion is assumed to be uniform across the tunnel face (Lee *et al.* 1992). Consequently, the modified gap parameter for the tunnel face is as follows

$$g_{face} = r_{eq} - r = \sqrt{\frac{\pi r^2 \cdot \frac{\delta_y}{\Delta y}}{\pi}} - r = r \cdot \left[\sqrt{\frac{\Delta y + \Delta y \left(\frac{\sigma_y - FP}{E_u} \right)}{\Delta y}} - 1 \right] = r \cdot \left[\sqrt{1 + \frac{\sigma_y - FP}{E_u}} - 1 \right] \quad (3)$$

where E_u is the undrained elastic modulus of the ground, δ_y is the unit ground intrusion and Δy is the unit advance of the shield.

The modified gap parameters of the shield annular gap and tail void were defined by considering the support characteristics. Based on the concept of the support characteristic curve on the convergence-confinement method (Carranza-Torres and Fairhurst 2000), the elastic radial deformation of the support annulus (u_r) can be derived elastically using the elastic stiffness of the support (K_s) and the external pressure (p_s) as follows

$$u_r = p_s / K_s \quad (4)$$

The elastic stiffness of the support is given by

$$K_s = \frac{E_s}{r(1+\upsilon_s)} \cdot \frac{r^2 - (r-t_s)^2}{r^2(1-2\upsilon_s) + (r-t_s)^2} \quad (5)$$

where E_s, t_s, and v_s denote the elastic modulus, thickness, and the Poisson's ratio of support material respectively. Thus, the modified gap parameters for the shield annular gap and tail void are derived as follows

$$g_{shield} = \frac{\sigma_{z,crown} - \sigma_{s1}}{\left(\frac{E_{s1}}{r(1+\upsilon_{s1})} \cdot \frac{r^2 - (r-t_{s1})^2}{r^2(1-2\upsilon_{s1}) + (r-t_{s1})^2} \right)} \quad (6)$$

$$g_{tail} = \frac{\sigma_{z,crown} - \sigma_{s2}}{\left(\frac{E_{s2}}{r(1+\upsilon_{s2})} \cdot \frac{r^2 - (r-t_{s2})^2}{r^2(1-2\upsilon_{s2}) + (r-t_{s2})^2} \right)} \quad (7)$$

where $\sigma_{z,crown}$ is the vertical total stress at the tunnel crown, s1 and s2 denotes the slurry injected on shield annular gap and grout injected on tail void respectively.

Previous researchers regarded that the volume loss around the tunnel equates to the area of the settlement trough at the surface. Thus, a linear relationship has been established between the sum of modified gap parameters for each construction phase and the maximum surface settlement, as represented by Eq. (2). Consequently, the predictive algorithm proposed in this study assumes that the maximum surface settlement is determined by the sum of modified gap parameters multiplied by ground correction coefficients α and β, as outlined in Eq. (8).

$$S_{max} = \alpha \times g_{face} + \beta \times [g_{shield} + g_{tail}] \quad (8)$$

Two different coefficients α and β are assigned: α for the face gap parameter, which is governed by active support, and β for the circumferential gap parameter, which are more influenced by the passive support provided by injected materials.

3. Numerical modeling

3.1 Finite difference model

The evaluation of ground correction coefficients was conducted using the results of numerical parametric analysis. Numerical analysis was performed using the commercial software FLAC3D (ver. 5.0, Itasca Consulting Group, Inc.) based on the finite difference method (FDM).

3.1.1 Modeling the ground

An appropriate domain size was selected for the numerical model, considering both the boundary effect and computational time. The minimum dimensions were proposed to be (H+3D) for the length (parallel to the tunnel axis), (H+4D) for the height, and 3H for the width (tunnel axis to boundary), where H is the depth of the tunnel springline and D is the tunnel diameter, based on a parametric study (Lambrughi *et al.* 2012). Fig. 3 illustrates the adopted model geometry ($120 \times 120 \times 60$ m), which meets the dimensional requirements for all validation cases and parametric analyses. A fully symmetry model composed of zone elements was adopted, and roller boundary

Table 1 Properties of structural elements and injected materials

Structural elements	Elastic modulus [MPa]	Poisson's ratio [-]	Density [kg/m^3]	Shear modulus [MPa]
Shield	200,000	0.25	7,840	80,000
Slurry for steering gap	0.0745	0.49	1,275	0.025
Grout at the terminal state	2,800	0.25	2,200	1,120

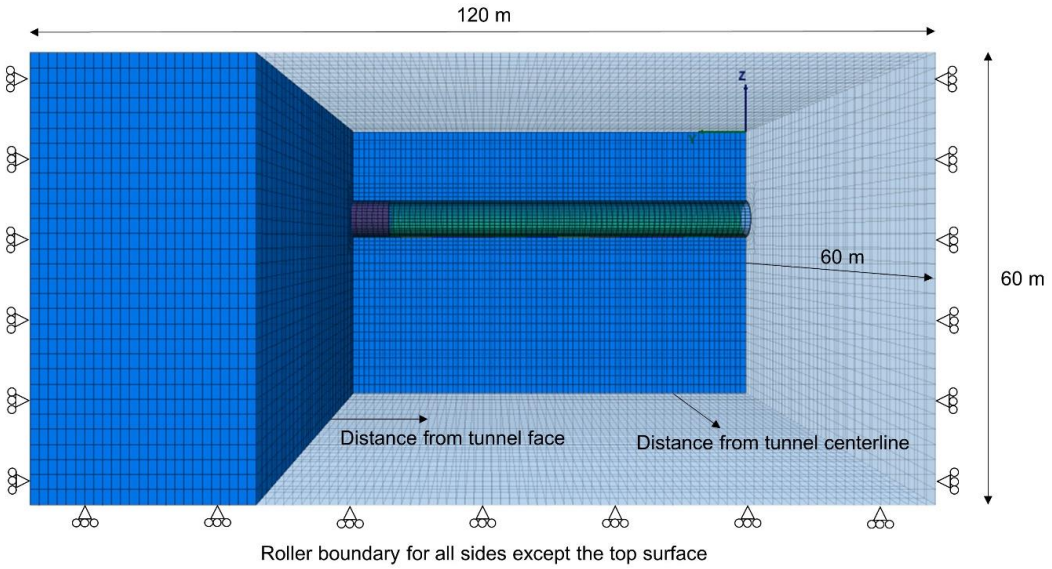

Fig. 3 Sketch of an adopted geometry

conditions, which constrain displacement normal to the boundary surface, were applied to all sides except for the free top surface. A zone size of approximately 0.8-1.2 m was applied near the tunnel, which was sufficient to capture stress redistribution and ground deformation in the surrounding ground (Lambrughi *et al*. 2012, Comodromos *et al.* 2014). The geotechnical properties were simulated by adopting the Mohr-Coulomb constitutive model, which describes a homogeneous and isotropic medium with linear elastic and perfectly plastic behaviors. The Mohr-Coulomb model is selected because it is widely applicable from general soils to rocks, and requires the least number of parameters compared with other advanced models such as the Drucker-Prager model or Hardening Soil model (Kratz *et al.* 2023). It is reasonable for the purpose of the study, as the developed model should be able to predict only commonly available geotechnical properties in order to perform its versatility at various sites. The initial stress equilibrium was achieved through iterative calculations until the mechanical unbalanced-to-applied force ratio dropped below 1e-05, following the assignment of ground properties and gravitational loading.

3.1.2 Modeling the shield TBM

The shield TBM was modeled using shell elements with a linear elastic model, which has been validated as a reliable model through previous numerical studies (Comodromos *et al*. 2014, Hasanpour *et al*. 2014). To simulate the shield annular gap, a linear elastic zone element was implemented around the shield, possessing a specified thickness. Essentially, the zone elements adjacent to the machine underwent nullification during excavation and were replaced with new zone elements characterized by the properties of bentonite slurry. It was assumed that slurry injection maintains a uniform radial pressure to the excavated surface until the TBM passed through. The pressure of slurry injection, denoted as *SP*, is described using a parameter known as the slurry injection pressure ratio (*SPR*). This ratio, expressed as Eq. (9), represents the relationship between *SP* and the horizontal earth pressure at rest on the center of the excavated face.

$$SPR = \frac{SP}{\sigma_h} = \frac{SP}{K_0 \sigma'_z + u} \tag{9}$$

The earth pressure coefficient at rest K_0, is empirically known to follow the following formula for the normally consolidated clay and granular soils (Jaky 1944)

$$K_0 = 1 - \sin\phi' \tag{10}$$

where the ϕ' is the internal friction angle. The elastic properties of the shield TBM and injected bentonite slurry are listed in Table 1.

3.1.3 Modeling the face pressure

The support for the tunnel face was modeled by applying a normal stress to the nodes located on the excavated tunnel face. The face pressure was selected to be a uniform value within the range extending from the active

earth pressure to the earth pressure at rest at the central point of the excavated face. The pressure applied on the excavated face corresponds to the total stress (Losacco and Viggiani 2019, Meschke *et al.* 2011, Ochmański *et al.* 2020). The description of face pressure is similar to those of SP and is articulated through the face pressure ratio (*FPR*), which represents the ratio between the face pressure and the horizontal earth pressure at rest on the center of the excavated face. Consequently, the FPR can be considered in a range of approximately 0.6 to 1.0 for excavations above the groundwater level and approximately 0.8 to 1.0 for excavations below the groundwater level, assuming an absence of a partially saturated medium at the initial condition. The range of FPR is reasonable by the Rankine's active earth pressure coefficient (K_a) expressed in Eq. (11), with considering the range of internal friction angles for geotechnical materials is universally between 0 and 45°.

$$K_a = \frac{1 - \sin\phi'}{1 + \sin\phi'} \tag{11}$$

In addition, the active state of the tunnel face experiences less pressure than Rankine's active pressure owing to longitudinal arching. Therefore, the appropriate range of the *FPR* value for shield tunneling is from 0.6 to 1.0.

3.1.4 Modeling the tail void grouting

In this numerical model, the shield TBM and segment lining were assumed to be coaxial with the excavation. Consequently, grouting was simulated to fill the tail void seamlessly. Upon advancement of the shield, the slurry material and its pressure were removed. Then, zone elements representing the grout were generated with corresponding properties and injection pressure. The grouting process was assumed to occur simultaneously with the shield's advance and hardened over time. The hardening behavior was regarded as the 'slowly hardening cement', following the *fib* Model Code for Concrete Structures 2010 (fib 2012), succeeding the CEB-FIP Model Code 1990 (CEB 1993), in alignment with the proposal by Comodromos *et al*. (2014). The simulation focused on the time-dependent increase in stiffness rather than on project-specific grout properties such as mix ratio or injection volume. For the sake of simplicity and computational efficiency, the representative grout hardening was discretely simulated. The average advance of the shield was regarded as six rings per 12 h and paused for 12 h. Thus, 27, 54, 66, 73, 78, 82, 85, 87, 89, 90, 91.5, and 92.5 % of the complete hardened modulus was applied at each of the six rings after injection. The terminal properties of the grout are detailed in Table 1. The injection pressure on the excavated surface was uniformly applied in the normal direction for up to six rings after injection, assuming an initial setting time of approximately 12 hours for the grouts. The injection pressure is recommended to be 100–200 kPa greater than the face pressure (KDS 2016), although this may vary in different field conditions. Consequently, the backfill injection pressure ratio (*BPR*), representing the ratio between the grout injection pressure and the total earth pressure at rest on the tunnel face center, was chosen within the range of 0 to 1.2 for the parametric studies in the numerical analysis.

3.1.5 Sequential simulation

After achieving initial equilibrium, the shield tunneling process was carried out iteratively in a sequential manner, as illustrated in Fig. 4. As illustrated in Fig. 4, the excavation and support process of the shield TBM is divided into two phases. During the first phase, corresponding to the right-hand loop in the figure, the model simulates shield advancement over a specified length (equal to the shield length) without installing the segment lining. In this stage, the simulation proceeds for n excavation cycles, in which excavation and face support are applied without tail void grouting. In the second phase, represented by the left-hand loop, segment lining and grouting are performed, and the simulation is continued to allow the surface settlement to converge. Once the total number of cycles reaches m, the simulation is terminated, and the final settlement troughs and maximum surface settlement value are obtained. Previous researchers have typically designated enough calculation steps for each advance and continuous support (An *et al*. 2022, Chakeri *et al.* 2013, Hasanpour 2014, Moeinossadat and Ahangari 2019). In this study, calculation of each advance and support was terminated when the unbalanced force ratio reaches 1e-05, aiming to minimize the number of steps for the entire sequence.

3.2 Validation of the numerical modeling

Validation of the numerical simulation was conducted using field measurements. All cases assumed the greenfield conditions. The results affirm that the numerical simulation constructed in this study is appropriate for obtaining a reliable analyses in the context of the parametric studies.

3.2.1 Validation for shield annular gap occurred by tunneling in soils

In-situ data measured during the construction of the Madrid Metro Extension Project were used to validate the numerical model of tunneling with the shield annular gap. The field data reported by Lambrughi *et al*. (2012) include surface settlement measurements obtained through SAI (Sistema de Auscultación Integrado), incorporating surface leveling and inclinometer readings during excavation. These data serve as the benchmark for validating the deformation pattern predicted in this study. The project employed an EPB (Earth Pressure Balanced) shield TBM with an excavation diameter of 9.38 m. The shield annular gap was assumed to be 0.03 m in thickness, which was determined by considering the overexcavation of the cutter head (Lambrughi *et al.* 2012). The groundwater table was disregarded due to the absence of a distinct water table, with several unconnected aquifers present. Numerical calculations were conducted for Section 8.2-4+310, where the excavation traverses mixed ground conditions. Depth of tunnel axis was 20.8 m. The ground properties for the specified sections are detailed in Table 2. As the literature does not provide specific information on the grout mix ratio or injection volume, the previously described grout

Table 2 Ground properties and profile of validation for shield annular gap occurred (modified from Lambrughi *et al.* 2012)

Depth [m]	Ground classification	Unit weight [kN/m^3]	Cohesion [kPa]	Internal friction angle [degree]	Elastic modulus [MPa]	Poisson's ratio [-]
0 – 13	Tosco arenoso (sandy clay)	20.8	105	31.7	123	0.3
13 – 16	Tosco (brown clay)	21	149	32.5	172	0.3
16 – 25.8	Tosco arenoso (sandy clay)	20.8	105	31.7	123	0.3
25.8 – 60	Tosco (brown clay)	21	149	32.5	172	0.3

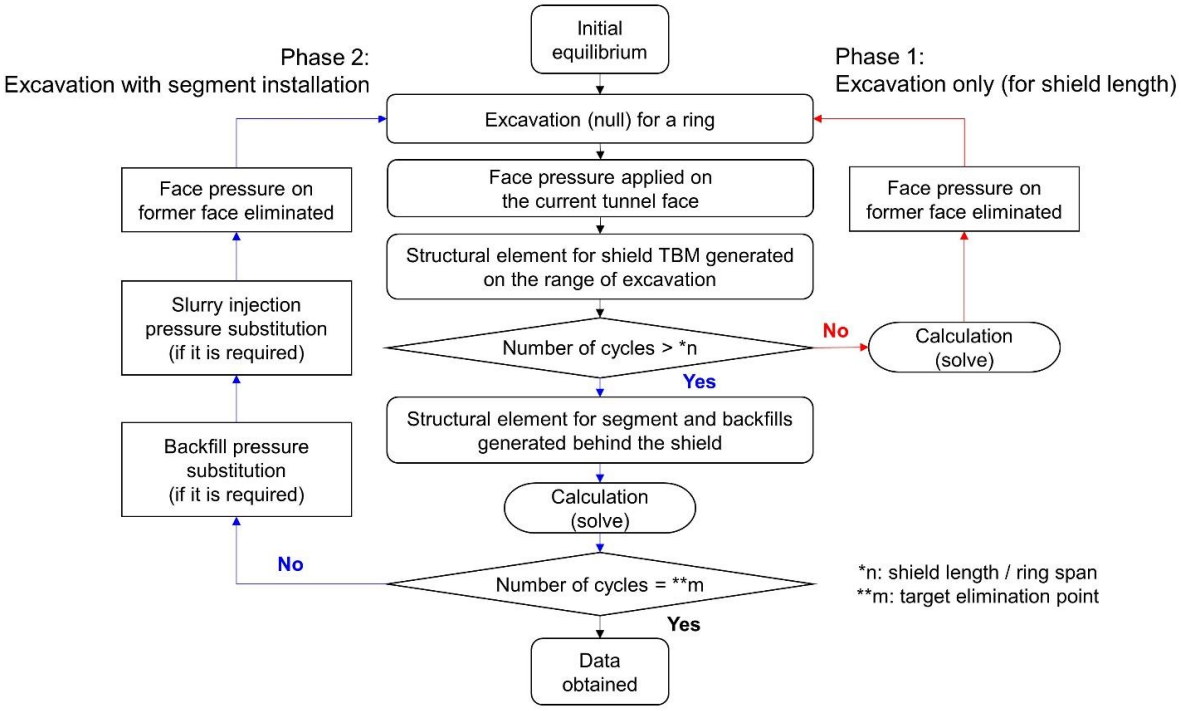

Fig. 4 Numerical procedures for simulating shield tunneling

properties were applied without further adjustment. According to values reported in the literature, the face pressure and gap grouting pressure were set to 100 kPa and 0 kPa, respectively. Since the slurry injection pressure for the shield annular gap was not specified in the literature, it was assumed to be equal to the gap grouting pressure.

Fig. 5 shows the contour of the vertical stress obtained for Section 8.2-4+310, highlighting key stages of excavation and support. At location [1], minor disturbance is observed in front of the tunnel face due to the applied face pressure, indicating the initial response of the ground prior to excavation. At point [2], over-excavation combined with insufficient injection pressure leads to a significant increase in vertical stress above the shield, resulting in concentrated load transfer to the surrounding ground. Finally at [3], after the installation of segmental lining, arching effects become apparent. The redistributed stress is transferred to the side of tunnel, resulting in vertical stress concentration adjacent to the tunnel boundary. This redistribution behavior confirms that the model captures the essential mechanisms of ground-structure interaction during shield tunneling. Fig. 6 illustrates the transverse surface settlement troughs resulting from the numerical modeling in this study, as well as the numerical calculations from a previous study and in-situ measured data. The concordance between these results supports the assertion that the numerical model developed in this study is reliable.

3.2.2 Validation for shield tunneling without shield annular gap

In-situ data measured during the construction of Tehran Metro Line 7 were used to validate the numerical modeling of tunneling without shield annular gap. In the Tehran Metro case, Chakeri *et al.* (2013) provided surface settlement records collected via optical markers installed along the tunnel alignment and nearby structures. These measurements were used to compare the predicted settlement trough in the present analysis. It is constructed

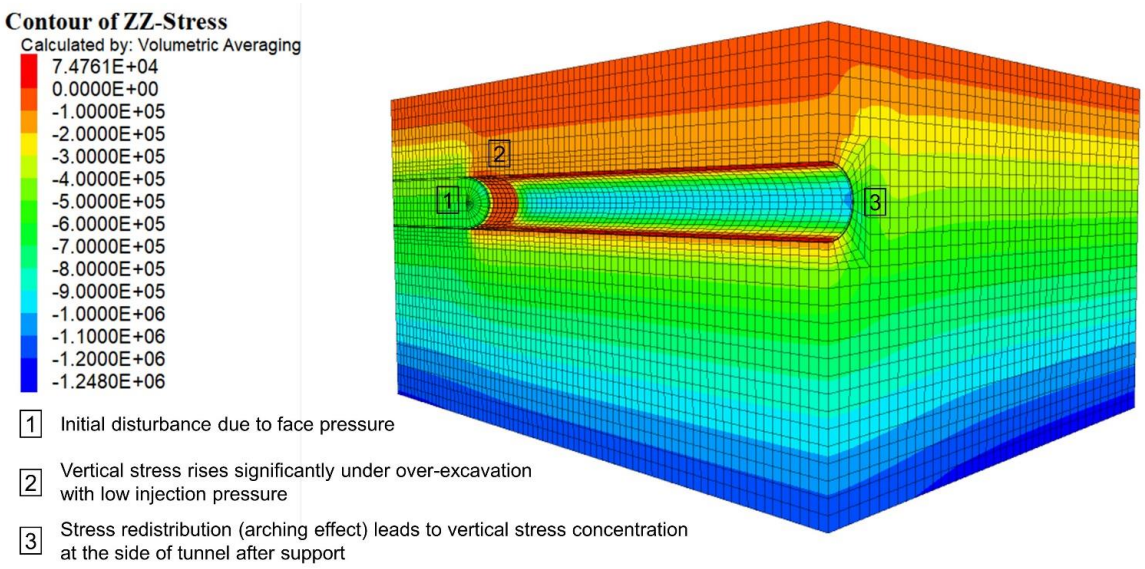

Fig. 5 Contour of vertical stress obtained for Madrid Metro Extension Project Section 8.2-4+310

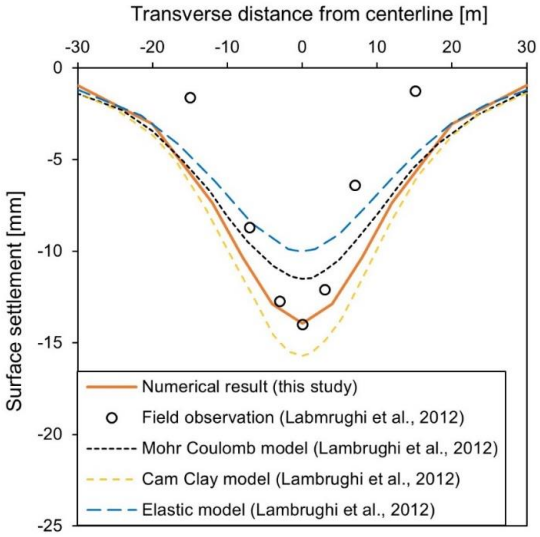

Fig. 6 Calculated and measured surface settlement in the cross-section of Madrid Metro Extension Project Section 8.2-4+310

using an EPB shield TBM with an excavation diameter of 9.2 m. No water seepage has occurred at this site. According to values reported in the literature, the face pressure was set to 55 kPa. Since the tail void grouting pressure was not specified in the literature, it was assumed to be equal to the face pressure. The sequence of the numerical simulation was similar to that in a previous study (An *et al*. 2022), except for the time-dependent hardening behavior of the grout and the advance rate.

In contrast to the previous case, Fig. 7 shows the vertical stress redistribution under conditions where the shield machine provides sufficient support without over-excavation. At [1], initial ground disturbance from the face pressure is observed, similar to the earlier case. However at [2], the development of vertical stress above the shield is substantially limited due to proper confinement during excavation. At [3], arching effect occurs after segment installation, but the overall stress concentration along the side of tunnel is more stable and symmetric. Fig. 8 presents the settlement troughs resulting from the numerical modeling in this study compared with the in-situ measured values. This indicates that the numerical model developed in this study is reliable.

4. Utilization of maximum settlement prediction algorithm

4.1 Numerical parametric results and analysis

A parametric analysis was conducted using the developed numerical modeling to evaluate the contribution of shield tunneling variables to the surface settlement and to investigate the support mechanisms of shield tunneling. The sensitivity of surface settlement to variations in the operational pressures (face pressure, slurry injection

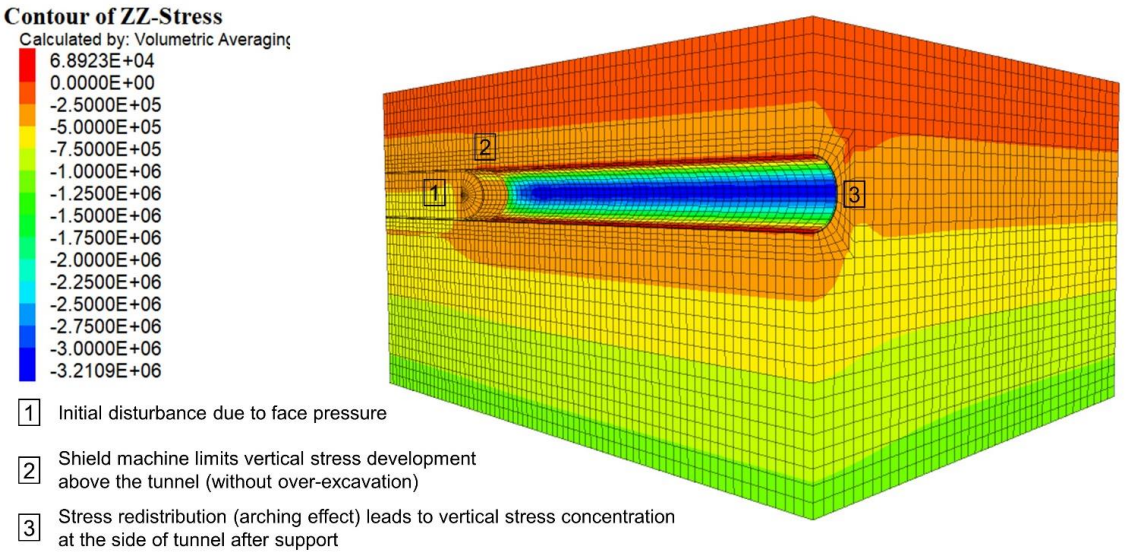

Fig. 7 Contour of vertical stress obtained for Tehran Metro Line 7

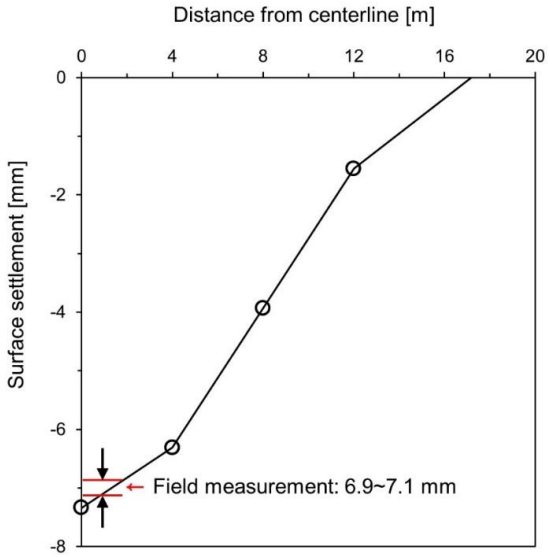

Fig. 8 Calculated and measured surface settlement in the cross-section of Tehran Metro Line 7

pressure to the shield annular gap, and backfill injection pressure to the tail void), presence of the shield annular gap, and elastic properties of the ground was examined. In line with previous recommendations, operational pressures were controlled by adjusting the ratios of pressures to the total horizontal earth pressure at the tunnel center, such as the *FPR*, *SPR*, and *BPR*, varied between 0.0 and 1.2. The tunnel axis was located at a depth of 20 m, and the excavation diameter was 8.4 m. For this parametric analysis, a shield annular gap thickness of 0.01 m, which is slightly larger than the typical range, was adopted to provide a conservative evaluation considering the steering and pitching. For the rock medium, the shield annular gap was considered to be negligible.

Based on geotechnical properties gathered from construction sites in South Korea, elastic properties showed significant correlation, as depicted in Fig. 9. Based on the in-situ properties, six types of ground were adopted for the parametric analysis as listed in Table 3. Each case was characterized by distinct elastic moduli (40 and 100 MPa, 2 and 8 GPa), and three Poisson's ratios (0.2, 0.3, 0.4) were applied at 40 MPa to examine the role of Poisson's ratio.

Fig. 10 presents the greenfield surface settlement troughs resulting from changes in Poisson's ratio while maintaining a constant elastic modulus of 40 MPa. Figs. 10(a) and 10(b) show the settlement troughs for identical support-pressure ratios. As Poisson's ratio decreased, horizontal confinement decreased, resulting in deeper and narrower settlement troughs. The inflection point of the trough, estimated using a Gaussian distribution curve, decreased as the Poisson's ratio decreased for the same stiffness and cohesion. The settlement trough parameter *K*, derived based on the inflection point over the depth of the tunnel center, was consistent with the empirical range (Mair

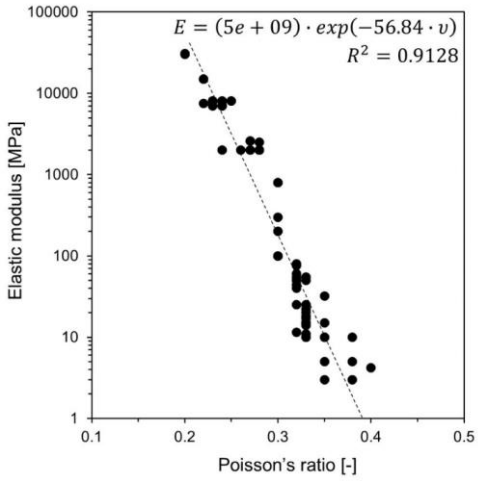

Fig. 9 Elastic properties collected from Korean in-situ field data

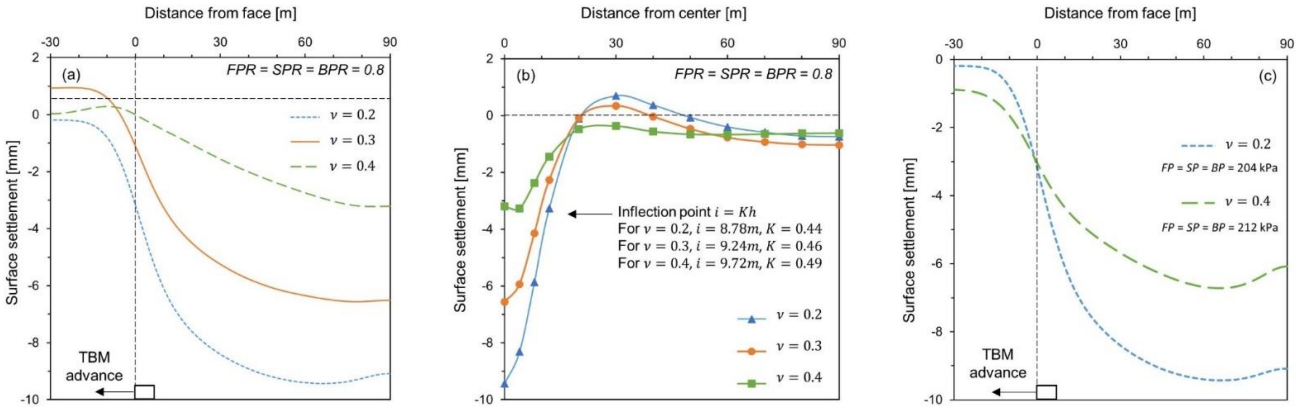

(a) Longitudinal troughs (b) Transverse troughs (c) Longitudinal troughs for a similar operation pressure values

Fig. 10 Calculated settlement with varying Poisson's ratios

Table 3 Geotechnical properties for parametric studies

Ground classification	Density [kg/m^3]	Cohesion [kPa]	Internal friction angle [degree]	Elastic modulus [MPa]	Poisson's ratio [-]
Soil #1	1,900	25	48.6	40	0.2
Soil #2	1,900	25	34.8	40	0.3
Soil #3	1,900	25	19.5	40	0.4
WR	2,100	30	33	100	0.3
SR	2,500	140	37	2,000	0.28
HR	2,800	1,000	45	8,000	0.25

Note. WR: weathered rock, SR: soft rock, HR: hard rock

and Taylor 1999). Fig. 10c shows the longitudinal troughs at similar support pressures. It indicates that increased confinement along the tunnel transfers stress to the adjacent medium, leading to smaller and broader ground deformation. A three-dimensional contour of vertical displacement for the case with Soil #3 is presented in Fig. 11 to visually complement the results in Fig. 10.

Fig. 12 presents greenfield surface settlement troughs resulting from variations in elastic modulus (100 MPa, 2 GPa, and 8 GPa) while changing geotechnical properties. Unlike the previous case, the inflection point increased with decreasing Poisson's ratio. It infers that larger stiffness and cohesion contribute more to arching development than the Poisson's ratio, restraining vertical movement of the ground above the tunnel through horizontal confinement.

The maximum surface settlement-to-face pressure ratio is displayed in Fig. 13. Fig. 13(a) shows results with varying Poisson's ratio for excavation with a shield annular

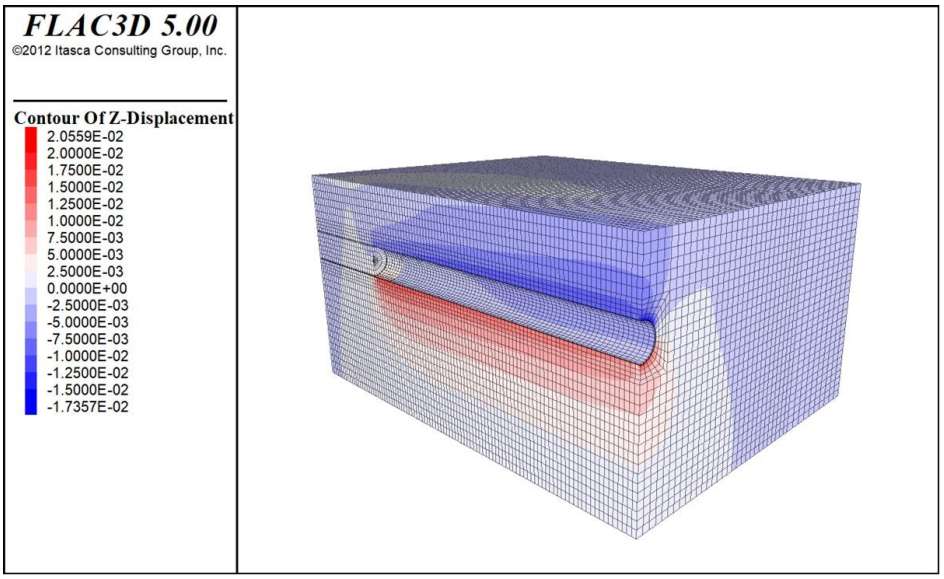

Fig. 11 Three-dimensional contour of vertical displacement for the case of Soil #3

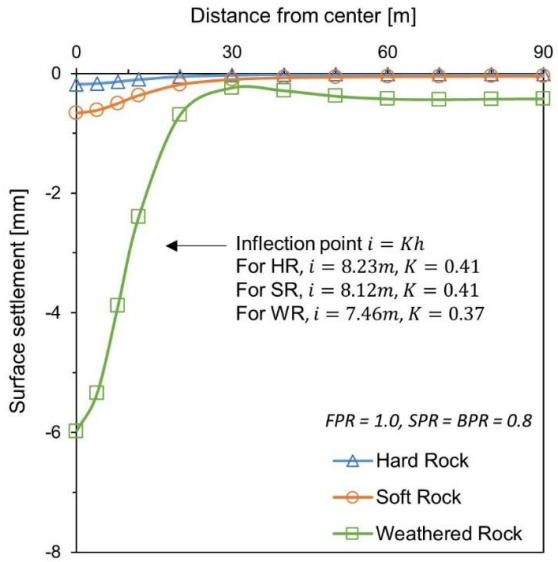

Fig. 12 Transverse settlement troughs by changing the elastic modulus

gap in the ground with a constant elastic modulus of 40 MPa. In all cases, the optimal *FPR* was approximately 0.8, resembling the active total earth pressure. Regardless of the Poisson's ratio, the pressure imbalance at the tunnel face led to similar maximum surface settlement values, indicating that settlement is ultimately dependent on ground stiffness. Fig. 13b shows the optimal *FPR* change based on the presence of a shield annular gap (over-cut). A hypothetical condition in which the support pressure was applied without a shield annular gap was simulated to compare the active and passive supports. The optimal *FPR* in the absence of slurry properties that are relatively weak compared to the ground is 1.0. Even with the same injection pressure, it is higher than the optimal *FPR* of 0.8 for the presence of slurry into shield annular gap. It is because the ground compresses and pressurizes the shield skin as the face pressure pushes the ground over the tunnel face.

Accordingly, the vertical deformation of the ground cannot be sufficiently compensated by weak support material. In other words, the passive support mechanism is more critical to the terminal value of the ground settlement.

Fig. 14 shows the maximum surface settlement resulting from slurry injection pressure on the shield annular gap during excavation in the ground with an elastic modulus of 40 MPa. Grout properties were applied to the tail voids, but the applied backfill injection pressure on the tail void was set to zero. The settlement decreased linearly in parallel with an increase in slurry injection pressure for different Poisson's ratios. It suggests that the deformation induced by injected slurry on the shield annular gap is governed by the support material property and is affected by the support pressure. In other words, the active support mechanism and passive support mechanism are activated simultaneously.

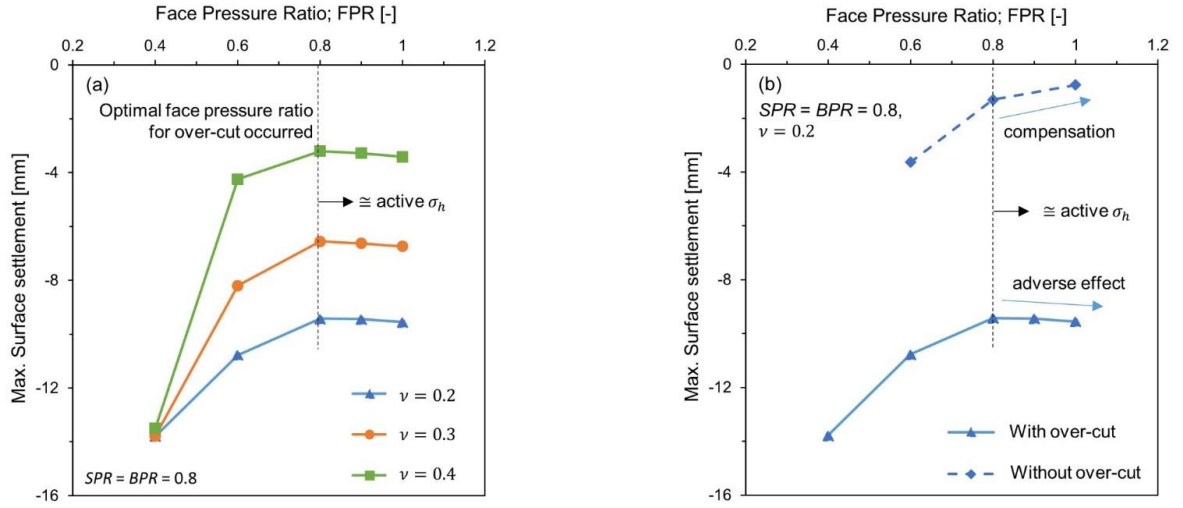

(a) with varying Poisson's ratio (b) with varying existence of shield annular gap

Fig. 13 Maximum surface settlement to the face pressure ratio

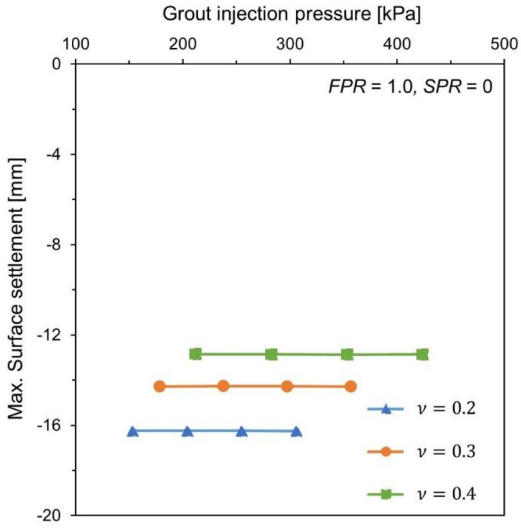

Fig. 14 Maximum surface settlement to the slurry injection pressure

Fig. 15 shows the maximum surface settlement when the slurry was substituted into the shield annular gap but no injection pressure was applied. Compared with Fig. 14, the grout injection pressure in the tail void did not significantly influence the surface settlement more than the slurry injection pressure in the shield annular gap. Additionally, maximum surface settlements for zero-*SPR* values were larger than those for zero-*BPR* values, indicating that higher stiffness of the supporting materials can more efficiently restrain settlement. It can be assumed that the passive support mechanism is fundamental in shield tunneling, with active support playing a supplementary and temporary role.

4.2 Determination of ground correction coefficients

The determination of ground correction coefficients was conducted using the numerical parametric results. From the proposed algorithm in Eq. (8), the modified gap parameter for the tail void (g_{tail}) should incorporate the elastic modulus at the initial setting time of the grout, which is only 27 % of the terminal value. It is because the grout into the tail void is regarded to lose its fluidity after the initial setting time, and is not able to perform active support afterwards. Coefficient β was determined by fitting the numerical data for *FPR* equal to 1.0, with a condition that renders coefficient α negligible. As implied by the parametric results, coefficient β exhibits a correlation with weaker supporting materials, such as slurry for the existence of a shield annular gap and grout. Fig. 16 presents the absolute values of β relative to the absolute values of modified gap parameters for various supporting materials. The gap parameter and its corresponding coefficients are negative when the injection pressure of the support material exceeds the total vertical earth pressure on the tunnel crown. Absolute values were used to describe the compression of the support material, making the direction of the imbalanced stress negligible. Clear power-law

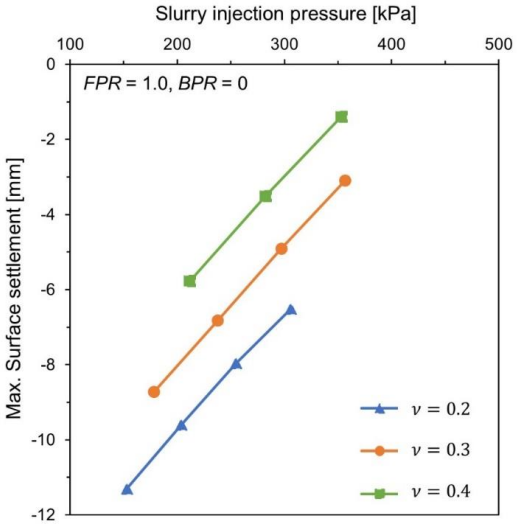

Fig. 15 Maximum surface settlement to the grout injection pressure

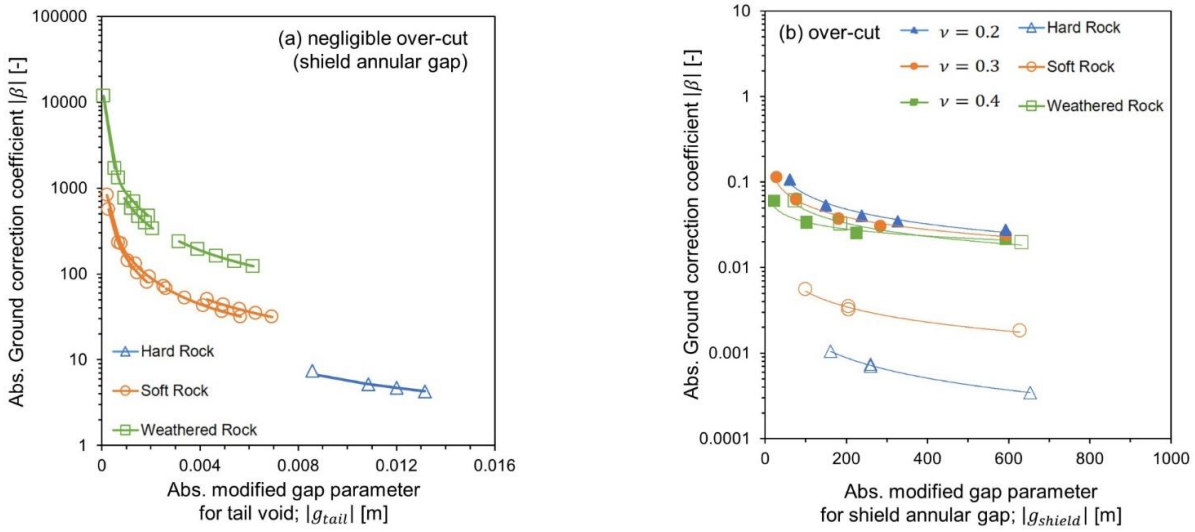

(a) for the grout injected on tail void (negligible over-cut) (b) for the slurry injected on shield annular gap (over-cut)

Fig. 16 Ground correction coefficient β to the modified gap parameter

correlations between β and modified gap parameters were established as listed in Table 4. These values approach zero for stiffer ground conditions. Fig. 17 presents coefficient α in relation to face pressure and modified gap parameters on the tunnel face for ground with a 40 MPa elastic modulus, because the ground loss at the tunnel face becomes negligible for stiff ground. Coefficient α cannot be derived when the face pressure is the same as the earth pressure at rest. Fig. 17(a) shows that α converges to the asymptotic value of -100 as the face pressure increases near the active earth pressure. This supports the fact that the plastic zone over the tunnel face occurs locally when the face pressure is controlled in the range of 60–65% of the active earth pressure (Anagnostou and Kovári 1996). The face pressure should exceed the pore pressure acting on the tunnel face. Fig. 17(b) shows the power function correlations between coefficient α and modified gap parameters, as listed in Table 4.

The linear formulation of the predictive algorithm enables the estimation of the contribution of each operational factor to the settlement, as illustrated in Fig. 18. While operational variables are not independent, the errors resulting from these coefficients are negligible. Consequently, the stiffness of the weaker support material is the dominant factor in maximum surface settlement unless the face pressure decreases below the active earth pressure.

5. Discussions

5.1 Applicability of prediction algorithm

To predict surface settlement accurately, various factors must be considered, including the excavation radius, tunnel center depth, elastic properties (elastic modulus and Poisson's ratio) of the ground and support materials,

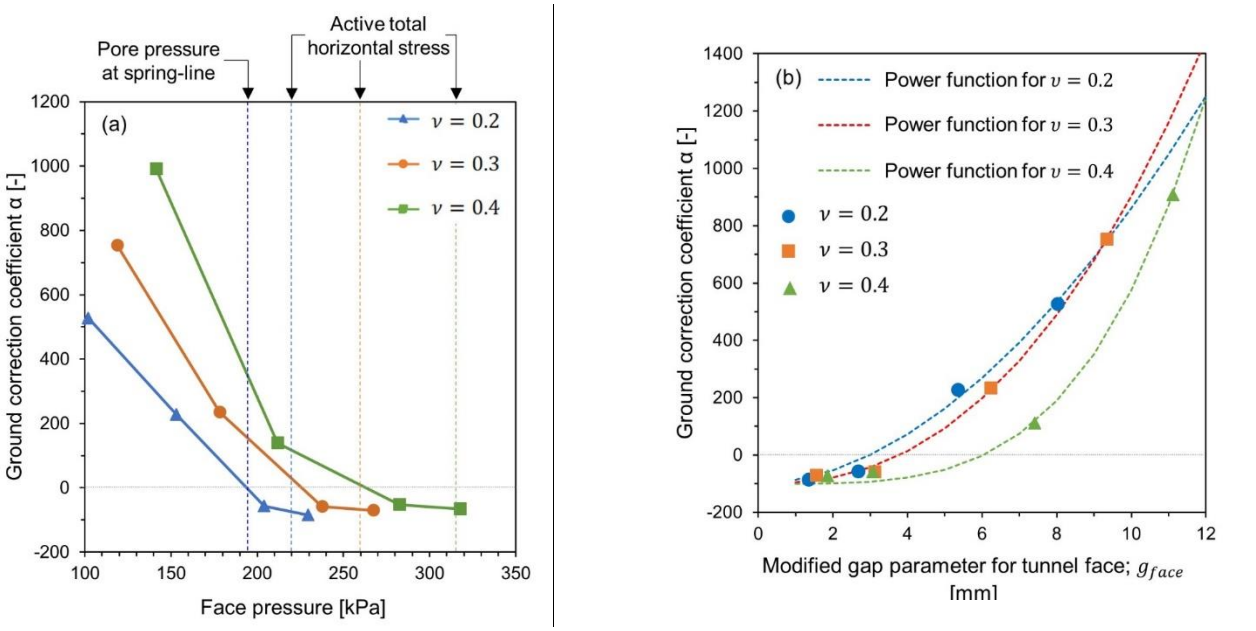

(a) to the face pressure (b) for the slurry injected on shield annular gap (over-cut)

Fig. 17 Ground correction coefficient α

Table 4 Power-function based correlation between modified gap parameters and ground correction coefficients

Ground correction coefficient	Soil (E = 40 MPa)			*WR* (E = 100 MPa)	*SR* (E = 2 GPa)	*HR* (E = 8 GPa)
	ν = 0.2	ν = 0.3	ν = 0.4			
$\lvert\beta\rvert$ for negligible over-cut	-	-	-	$0.57 \cdot \lvert g_{tail}\rvert^{-1.05}$	$0.30 \cdot \lvert g_{tail}\rvert^{-0.92}$	$0.015 \cdot \lvert g_{tail}\rvert^{-1.30}$
$\lvert\beta\rvert$ for over-cut exist	$1.03 \cdot \lvert g_{shield}\rvert^{-0.58}$	$0.50 \cdot \lvert g_{shield}\rvert^{-0.48}$	$0.12 \cdot \lvert g_{shield}\rvert^{-0.27}$	$0.50 \cdot \lvert g_{shield}\rvert^{-0.51}$	$0.083 \cdot \lvert g_{shield}\rvert^{-0.6}$	$0.056 \cdot \lvert g_{shield}\rvert^{-0.79}$
α	$12.8 \cdot (g_{face})^{-1.87} - 100$	$4.18 \cdot (g_{face})^{-2.38} - 100$	$0.11 \cdot (g_{face})^{-3.79} - 100$	-	-	-

Note. E (elastic modulus), ν (Poisson's ratio), | | (absolute value)

thickness of the injected support materials, face pressure, total horizontal earth pressure, pore pressure at the tunnel spring line, and support injection pressure. Fig. 19 provides a schematic representation of settlement prediction and data-gathering points. Geotechnical properties are collected before construction, and facial conditions are obtained during excavation. However, properties related to the injection of support materials are determined a few rings behind, where ground deformation has already occurred. Therefore, in the design phase, the predictive system uses predetermined values as listed in Table 1 for these vacant parameters. In summary, the only essential real-time inputs required at the prediction point are the ground properties and face pressure, making the algorithm particularly applicable during early-stage planning and excavation.

To validate the developed algorithm, it is crucial to compare predicted maximum surface settlement values with field-obtained results. There are few sites of undrained tunneling that have documented records of support material properties and injection pressures. The prediction algorithm was applied and assessed based on data from the East Side Access Queens Bored Tunnels (Grasmick *et al.* 2015). The tunnel, excavated using a 6.9 m slurry shield TBM, had a springline depth of 22.77 m. The ground was sandy soil and assumed homogeneous with properties listed in Table 5 (Mooney *et al.* 2016). The shield annular gap thickness was 0.04 m, and the tail void thickness was assumed to be 0.15 m. Slurry injection pressure along the shield annular gap and grout injection pressure onto the tail void were approximately 0.7 and 1.5 times the vertical total earth pressure at the tunnel springline, respectively. Using representative elastic properties of the slurry and grout from the parametric studies, the predicted maximum surface settlement was 7.78 mm. This prediction was considered reliable when compared with field-obtained data ranging from 6 to 8 mm.

Furthermore, the prediction algorithm was applied to the Madrid Metro Extension Project (Lambrughi *et al.* 2012), focusing on sections where face pressure and maximum surface settlement were measured. The influence of face pressure and grout injection pressure on the tail void was

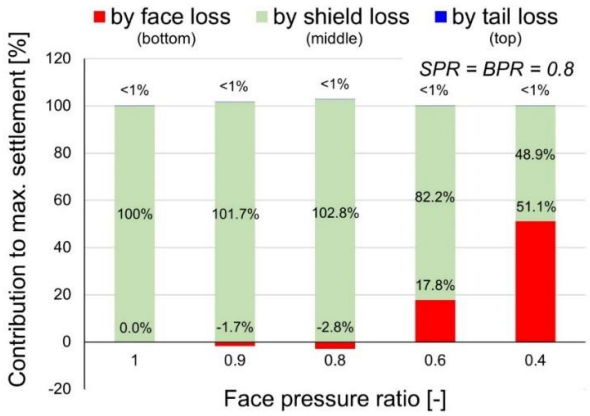

Fig. 18 Contribution of shield TBM operational factors to the maximum surface settlement

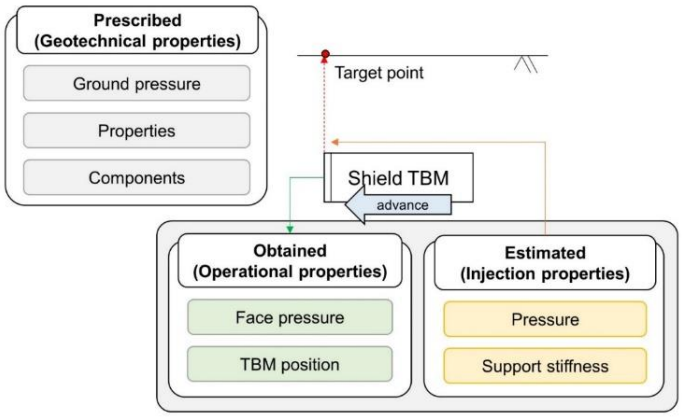

Fig. 19 Data required to run the predictive algorithm and their collecting point

found to be insignificant, as discussed in the previous parametric analysis. Predictions for maximum surface settlement, when the slurry injection pressure onto the shield annular gap was 0.75 times the vertical total earth pressure at the tunnel crown, were in close agreement with measured values for Sections 4.2-2+526, 8.2-4+310, and 9.2+260, at 12.04, 14.04, and 11.88 mm, respectively, compared to measured values of 12, 14, and 13 mm. In conclusion, the developed prediction algorithm demonstrates high accuracy in determining maximum surface settlement for undrained shield tunneling, utilizing a small number of variables.

Compared to empirical models (e.g., Peck 1969, O'Reilly and New 1982), which rely on simplified geometric relationships and volume loss assumptions, the present algorithm accounts for both ground stiffness and support conditions. Analytical models (e.g., Loganathan and Poulos 1998) improve on this by including elastic ground response and face pressure effects, but still lack resolution in modeling support-material interactions. Full-scale numerical simulations offer detailed predictions but are computationally intensive and require considerable time. In contrast, the proposed algorithm uses a simplified linear formulation while retaining physical transparency through the use of correction coefficients α and β, which quantify the distinct roles of active and passive support.

Furthermore, when compared to machine learning-based approaches (e.g., Kim *et al*. 2022), which require large site-specific datasets to construct a model, the proposed algorithm achieves comparable predictive accuracy with minimal inputs and clearer physical meaning. This balance between computational efficiency, mechanistic clarity, and verified accuracy distinguishes the algorithm as a practical and novel approach to predicting shield tunneling-induced surface settlement.

5.2 Limitations and future work

While the proposed prediction algorithm demonstrates strong applicability and accuracy during the construction, several limitations should be acknowledged. First, the current modeling framework assumes undrained conditions of the ground, without considering pore pressure dissipation or groundwater inflow. Although this assumption is valid for short-term excavation in low-permeability soils, it may not accurately capture settlement behavior in more permeable strata. Future research could improve the model by incorporating a groundwater-influenced gap parameter, enabling predictions that reflect seepage-related deformation.

Second, the model simplifies face pressure as a unified reaction force at the tunnel face, without distinguishing the

Table 5 Geotechnical properties of sandy soil representing the East Side Access Queens Bored Tunnels (modified from Mooney *et al*. 2016)

Unit weight [kN/m^3]	Internal friction angle [degree]	Elastic modulus [MPa]	Poisson's ratio [-]
20	40	200	0.3

underlying mechanisms specific to different shield types. In EPB shield tunneling, for example, chamber pressure is influenced by thrust force, screw conveyor performance, volume of discharged muck. In slurry shields, slurry infiltration pressure can diverge from the net ground pressure at tunnel face. These distinctions are not explicitly represented in the current algorithm. A future extension of this work could involve deriving face pressure from actual machine operation data, enabling better adaptation to specific shield systems.

Beyond these two key limitations, the model also assumes idealized boundary conditions for slurry and grout injection, excluding dissipation, pore pressure development, or coupled fluid-soil interaction. Moreover, although the prediction algorithm was validated using well-documented case studies, direct validation with new project-specific monitoring data would further enhance confidence in its generalizability.

Despite these limitations, the algorithm remains robust for applications, particularly in scenarios where undrained behavior dominates. Its modular structure offers flexibility for future enhancement, including the integration of advanced rheological models, real-time TBM machine data, or hybrid learning frameworks. These extensions will enable broader applicability while preserving the model's interpretability and computational efficiency.

6. Conclusions

This study proposed a simple and practical prediction algorithm for the maximum surface settlement induced by shield tunneling. This work particularly sheds light on the following key findings.

- A predictive algorithm was formulated based on parametric results from three-dimensional numerical analysis. Proposed algorithm incorporated gap parameters at the tunnel face, shield annular gap, and tail void. These were modified using stress states and support stiffness concepts. Correction coefficients were derived to represent support-phase contributions at specific ground type.
- Parametric results demonstrated that the stiffness of the weaker support material is the dominant factor in controlling surface settlement, unless face pressure drops below the active earth pressure. Passive support mechanisms were found to play a more crucial role than active support.
- The proposed algorithm enables accurate estimation of maximum settlement using a limited number of variables, primarily ground properties and face pressure.
- Field data were used to validate the numerical modeling and algorithm. Predicted settlement values showed strong agreement with measured data, with errors less than 2 mm.
- Compared to empirical or data-driven models, the algorithm offers enhanced interpretability, better incorporation of support mechanisms, and improved efficiency for field applications.
- The current model assumes undrained conditions and generalized support behavior. Future research may extend the framework to include groundwater infiltration, time-dependent consolidation, and machine-specific inputs for EPB or slurry TBMs.

Acknowledgments

This work is supported by "Ministry of the Interior and Safety" R&D program (20018374).

References

An, J.B., Kang, S.J., Kim, J. and Cho, G.C. (2022), "Numerical evaluation of surface settlement induced by ground loss from the face and annular gap of EPB shield tunneling", *Geomech. Eng.*, **29**(3), 291-300. https://doi.org/10.12989/gae.2022.29.3.291.

Anagnostou, G. and Kovári, K. (1996), "Face stability conditions with earth-pressure-balanced shields", *Tunn. Undergr. Sp. Tech.*, **11**(2), 165-173. https://doi.org/10.1016/0886-7798(96)00017-X.

Attewell, P. and Farmer, I. (1974), "Ground deformations resulting from shield tunnelling in London Clay", *Can. Geotech. J.*, **11**(3), 380-395. https://doi.org/10.1139/t74-039.

Carranza-Torres, C. and Fairhurst, C. (2000), "Application of the convergence-confinement method of tunnel design to rock masses that satisfy the Hoek-Brown failure criterion", *Tunn. Undergr. Sp. Tech.*, **15**(2), 187-213. https://doi.org/10.1016/S0886-7798(00)00046-8.

CEB (1993), "CEB-FIP Model Code 1990 CEB Bulletin D'Information No. 213/214, Comite Euro-International du Beton, Lausanne.

Chakeri, H., Ozcelik, Y. and Unver, B. (2013), "Effects of important factors on surface settlement prediction for metro tunnel excavated by EPB", *Tunn. Undergr. Sp. Tech.*, **36**, 14-23. https://doi.org/10.1016/j.tust.2013.02.002.

Chapman, D., Ahn, S. and Hunt, D.V. (2007), "Investigating ground movements caused by the construction of multiple tunnels in soft ground using laboratory model tests", *Can. Geotech. J.*, **44**(6), 631-643. https://doi.org/10.1139/t07-018.

Chen, R.P., Zhang, P., Kang, X., Zhong, Z.Q., Liu, Y. and Wu, H.N. (2019), "Prediction of maximum surface settlement caused by earth pressure balance (EPB) shield tunneling with ANN methods", *Soils Found.*, **59**(2), 284-295. https://doi.org/10.1016/j.sandf.2018.11.005.

Comodromos, E.M., Papadopoulou, M.C. and Konstantinidis, G.K. (2014), "Numerical assessment of subsidence and adjacent building movements induced by TBM-EPB tunneling", *J. Geotech. Geoenviron. Eng.*, **140**(11), 04014061. https://doi.org/10.1061/(ASCE)GT.1943-5606.0001166.

Dalong, J., Xiang, S. and Dajun, Y. (2020), "Theoretical analysis of three-dimensional ground displacements induced by shield tunneling", *Appl. Math. Model.*, **79**, 85-105. https://doi.org/10.1016/j.apm.2019.10.014.

fib (2012), "Model Code 2010", fib Bulletin No. 65/66, Federation internationale du beton, Lausanne.

Freitag, S., Cao, B.T., Ninić, J. and Meschke, G. (2018), "Recurrent neural networks and proper orthogonal decomposition with interval data for real-time predictions of mechanised tunnelling processes", *Comput. Struct*., **207**, 258-273. https://doi.org/10.1016/j.compstruc.2017.03.020.

Goh, A.T.C., Zhang, W., Zhang, Y., Xiao, Y. and Xiang, Y. (2018), "Determination of earth pressure balance tunnel-related maximum surface settlement: a multivariate adaptive regression splines approach", *Bull. Eng. Geol. Environ*., 77, 489-500. https://doi.org/10.1007/s10064-016-0937-8.

Grasmick, J., Rysdahl, B., Mooney, M., Robinson, B., Prantil, E., and Thompson, A. (2015), "Evaluation of slurry TBM design support pressures using east side access Queens bored tunnels data", Proc., Rapid Excavation and Tunneling Conference (RETC).

Hasanpour, R. (2014), "Advance numerical simulation of tunneling by using a double shield TBM", *Comput. Geotech.*, **57**, 37-52. https://doi.org/10.1016/j.compgeo.2014.01.002.

Hasanpour, R., Rostami, J. and Ünver, B. (2014), "3D finite difference model for simulation of double shield TBM tunneling in squeezing grounds", *Tunn. Undergr. Sp. Tech*., **40**, 109-126. https://doi.org/10.1016/j.tust.2013.09.012.

Jacobsz, S.W. (2002), "The effects of tunnelling on piled foundations", PhD thesis, University of Cambridge.

Jaky, J. (1944), "The coefficient of earth pressure at rest", *J. Soc. Hungarian Architects and Engineers*.

Karniadakis, G.E., Kevrekidis, I.G., Lu, L., Perdikaris, P., Wang, S. and Yang, L. (2021), "Physics-informed machine learning", *Nat. Rev. Phys*., **3**(6), 422-440. https://doi.org/10.1038/s42254-021-00314-5.

Kasper, T. and Meschke, G. (2004), "A 3D finite element simulation model for TBM tunnelling in soft ground", *Int. J. Numer. Anal. Method. Geomech*., **28**(14), 1441-1460. https://doi.org/10.1002/nag.395.

Kasper, T. and Meschke, G. (2006a), "On the influence of face pressure, grouting pressure and TBM design in soft ground tunnelling", *Tunn. Undergr. Sp. Tech*., **21**(2), 160-171. https://doi.org/10.1016/j.tust.2005.06.006.

Kasper, T. and Meschke, G. (2006b), "A numerical study of the effect of soil and grout material properties and cover depth in shield tunnelling", *Comput. Geotech*., **33**(4-5), 234-247. https://doi.org/10.1016/j.compgeo.2006.04.004.

KDS (2016), "TBM (KDS 27 25 00)", Korea Construction Standards Center, Republic of Korea.

Kim, C., Bae, G., Hong, S., Park, C., Moon, H. and Shin, H. (2001), "Neural network based prediction of ground surface settlements due to tunnelling", *Comput. Geotech*., **28**(6-7), 517-547. https://doi.org/10.1016/S0266-352X(01)00011-8.

Kim, D., Kwon, K., Pham, K., Oh, J.Y. and Choi, H. (2022), "Surface settlement prediction for urban tunneling using machine learning algorithms with Bayesian optimization", *Automat. Constr*., **140**, 104331. https://doi.org/10.1016/j.autcon.2022.104331.

Kratz, B., Jehel, P. and Tatin, M. (2023), "3D numerical simulation of TBM excavation for predicting surface settlements-state of the art", Expanding Underground-Knowledge and Passion to Make a Positive Impact on the World, 2757-2765.

Lambrughi, A., Rodríguez, L.M. and Castellanza, R. (2012), "Development and validation of a 3D numerical model for TBM–EPB mechanised excavations", *Comput. Geotech*., **40**, 97-113. https://doi.org/10.1016/j.compgeo.2011.10.004.

Lee, K., Rowe, R.K. and Lo, K. (1992), "Subsidence owing to tunnelling. I. Estimating the gap parameter", *Can. Geotech. J*., **29**(6), 929-940. https://doi.org/10.1139/t92-104.

Loganathan, N. (2011), An innovative method for assessing tunnelling-induced risks to adjacent structures, Parsons Brinckerhoff Incorporated New York, NY, USA.

Loganathan, N. and Poulos, H. (1998), "Analytical prediction for tunneling-induced ground movements in clays", *J. Geotech. Geoenviron. Eng*., **124**(9), 846-856. https://doi.org/10.1061/(ASCE)1090-0241(1998)124:9(846).

Losacco, N. and Viggiani, G.M. (2019), "Class A prediction of mechanised tunnelling in Rome", *Tunn. Undergr. Sp. Tech*., **87**, 160-173. https://doi.org/10.1016/j.tust.2019.02.020.

Mair, R. and Taylor, R. (1999), "Bored tunnelling in the urban environments", *Proceedings of the 14th International Conference on Soil Mechanics and Foundation Engineering. Proceedings International Society for Soil Mechanics and Foundation Engineering*.

Mair, R., Taylor, R. and Bracegirdle, A. (1993), "Subsurface settlement profiles above tunnels in clays", *Geotechnique*, **43**(2), 315-320. https://doi.org/10.1680/geot.1993.43.2.315.

Marshall, A., Farrell, R., Klar, A. and Mair, R. (2012), "Tunnels in sands: the effect of size, depth and volume loss on greenfield displacements", *Géotechnique*, **62**(5), 385-399. https://doi.org/10.1680/geot.10.P.047.

Meschke, G., Nagel, F. and Stascheit, J. (2011), "Computational simulation of mechanized tunneling as part of an integrated decision support platform", *Int. J. Geomech*., **11**(6), 519-528. https://doi.org/10.1061/(ASCE)GM.1943-5622.0000044.

Moeinossadat, S.R. and Ahangari, K. (2019), "Estimating maximum surface settlement due to EPBM tunneling by Numerical-Intelligent approach–A case study: Tehran subway line 7", *Transport. Geotech*., **18**, 92-102. https://doi.org/10.1016/j.trgeo.2018.11.009.

Mooney, M.A., Grasmick, J., Kenneally, B. and Fang, Y. (2016), "The role of slurry TBM parameters on ground deformation: Field results and computational modelling", *Tunn. Undergr. Sp. Tech*., **57**, 257-264. https://doi.org/10.1016/j.tust.2016.01.007.

Mroueh, H. and Shahrour, I. (2008), "A simplified 3D model for tunnel construction using tunnel boring machines", *Tunn. Undergr. Sp. Tech*., **23**(1), 38-45. https://doi.org/10.1016/j.tust.2006.11.008.

Nomoto, T., Imamura, S., Hagiwara, T., Kusakabe, O. and Fujii, N. (1999), "Shield tunnel construction in centrifuge", *J. Geotech. Geoenviron. Eng*., **125**(4), 289-300. https://doi.org/10.1061/(ASCE)1090-0241(1999)125:4(289).

O'Reilly, M.P. and New, B. (1982), Settlements above tunnels in the United Kingdom-their magnitude and prediction.

Ochmański, M., Modoni, G. and Bzówka, J. (2018), "Automated numerical modelling for the control of EPB technology", *Tunn. Undergr. Sp. Tech*., **75**, 117-128. https://doi.org/10.1016/j.tust.2018.02.006.

Ochmański, M., Spacagna, R.L. and Modoni, G. (2020), "3D numerical simulation of consolidation induced in soft ground by EPB technology and lining defects", *Comput. Geotech*., **128**, 103830. https://doi.org/10.1016/j.compgeo.2020.103830.

Peck, B. (1969), "Deep excavation and tunnelling in soft ground, State of the art volume", *Proceedings of the 7th ICSMFE*.

Phoon, K.K. and Zhang, W. (2023), "Future of machine learning in geotechnics", Georisk: Assessment and Management of Risk for Engineered Systems and Geohazards, **17**(1), 7-22. https://doi.org/10.1080/17499518.2022.2087884.

Ramoni, M. and Anagnostou, G. (2010), "Tunnel boring machines under squeezing conditions", *Tunn. Undergr. Sp. Tech*., **25**(2), 139-157. https://doi.org/10.1016/j.tust.2009.10.003.

Reichstein, M., Camps-Valls, G., Stevens, B., Jung, M., Denzler, J., Carvalhais, N. and Prabhat, F. (2019), "Deep learning and process understanding for data-driven Earth system science", *Nature*, **566**(7743), 195-204. https://doi.org/10.1038/s41586-019-0912-1.

Repetto, L. and Fidelibus, C. (2017), "Decision Plots for preliminary design of single-shield TBMs", *Eng. Geol*., **216**, 134-139. https://doi.org/10.1016/j.enggeo.2016.11.023.

Rowe, R. and Lee, K. (1992), "An evaluation of simplified techniques for estimating three-dimensional undrained ground movements due to tunnelling in soft soils", *Can. Geotech. J*,, **29**(1), 39-52. https://doi.org/10.1139/t92-005.

Santos Jr, O.J. and Celestino, T.B. (2008), "Artificial neural networks analysis of Sao Paulo subway tunnel settlement data", *Tunn. Undergr. Sp. Tech*., **23**(5), 481-491. https://doi.org/10.1016/j.tust.2007.07.002.

Selby, A. (1988), "Surface movements caused by tunnelling in two-layer soil", Geological Society, London, Engineering Geology Special Publications, **5**(1), 71-77.

Standing, J. and Selemetas, D. (2013), "Greenfield ground response to EPBM tunnelling in London Clay", *Géotechnique*, **63**(12), 989-1007. https://doi.org/10.1680/geot.12.P.154.

Sugiyama, T., Hagiwara, T., Nomoto, T., Nomoto, M., Ano, Y., Mair, R., Bolton, M. and Soga, K. (1999), "Observations of ground movements during tunnel construction by slurry shield method at the Docklands Light Railway Lewisham Extension-East London", *Soils Found*., **39**(3), 99-112. https://doi.org/10.3208/sandf.39.3_99.

Suwansawat, S. and Einstein, H.H. (2006), "Artificial neural networks for predicting the maximum surface settlement caused by EPB shield tunneling", *Tunn. Undergr. Sp. Tech*., **21**(2), 133-150. https://doi.org/10.1016/j.tust.2005.06.007.

Suwansawat, S. and Einstein, H.H. (2007), "Describing settlement troughs over twin tunnels using a superposition technique", *J. Geotech. Geoenviron. Eng*., **133**(4), 445-468. https://doi.org/10.1061/(ASCE)1090-0241(2007)133:4(445).

Verruijt, A. and Booker, J. (1996), "Surface settlements due to deformation of a tunnel in an elastic half plane", *Géotechnique*, **46**(4), 753-756.

Wan, M., Standing, J., Potts, D. and Burland, J. (2017), "Measured short-term ground surface response to EPBM tunnelling in London Clay", *Géotechnique*, **67**(5), 420-445. https://doi.org/10.1680/jgeot.16.P.099.

Xiang, Y., Liu, H., Zhang, W., Chu, J., Zhou, D. and Xiao, Y. (2018), "Application of transparent soil model test and DEM simulation in study of tunnel failure mechanism", *Tunn. Undergr. Sp. Tech*., **74**, 178-184. https://doi.org/10.1016/j.tust.2018.01.020.

Zhang, N., Zhou, A., Pan, Y. and Shen, S.L. (2021b), "Measurement and prediction of tunnelling-induced ground settlement in karst region by using expanding deep learning method", *Measurement*, **183**, 109700. https://doi.org/10.1016/j.measurement.2021.109700.

Zhang, P., Wu, H.N., Chen, R.P., Dai, T., Meng, F.Y. and Wang, H.B. (2020), "A critical evaluation of machine learning and deep learning in shield-ground interaction prediction", *Tunn. Undergr. Sp. Tech*., **106**, 103593. https://doi.org/10.1016/j.tust.2020.103593.

Zhang, W., Li, H., Li, Y., Liu, H., Chen, Y. and Ding, X. (2021a), "Application of deep learning algorithms in geotechnical engineering: a short critical review", *Artif. Intell. Rev.*, 1-41. https://doi.org/10.1007/s10462-021-09967-1.

Zhao, K., Janutolo, M. and Barla, G. (2012), "A completely 3D model for the simulation of mechanized tunnel excavation", *Rock Mech. Rock Eng*., **45**, 475-497. https://doi.org/10.1007/s00603-012-0224-3.

Zhou, X., Zhao, C. and Bian, X. (2023), "Prediction of maximum ground surface settlement induced by shield tunneling using XGBoost algorithm with golden-sine seagull optimization", *Comput. Geotech*., **154**, 105156. https://doi.org/10.1016/j.compgeo.2022.105156.

IC